

RESEARCH

Open Access



Wnt7a is required for regeneration of dystrophic skeletal muscle

Uxia Gurriaran-Rodriguez^{1,2,4}, Kasun Kodippili^{1,2}, David Datzkiw^{1,2}, Ehsan Javandoost^{1,2}, Fan Xiao^{1,2}, Maria Teresa Rejas³ and Michael A. Rudnicki^{1,2*}

Abstract

Intramuscular injection of Wnt7a has been shown to accelerate and augment skeletal muscle regeneration and to ameliorate dystrophic progression in *mdx* muscle, a model for Duchenne muscular dystrophy (DMD). Here, we assessed muscle regeneration and function in wild type (WT) and *mdx* mice where Wnt7a was deleted in muscle using a conditional *Wnt7a* floxed allele and a *Myf5-Cre* driver. We found that both WT and *mdx* mice lacking Wnt7a in muscle, exhibited marked deficiencies in muscle regeneration at 21 d following cardiotoxin (CTX) induced injury. Unlike WT, deletion of Wnt7a in *mdx* resulted in decreased force generation prior to CTX injury. However, both WT and *mdx* muscle lacking Wnt7a displayed decreased force generation following CTX injection. Notably the regeneration deficit in *mdx* mice was rescued by a single tail vein injection of extracellular vesicles containing Wnt7a (Wnt7a-EVs). Therefore, we conclude that the regenerative capacity of muscle in *mdx* mice is highly dependant on the upregulation of endogenous Wnt7a following injury, and that systemic delivery of Wnt7a-EVs represents a therapeutic strategy for treating DMD.

Keywords Skeletal muscle, Regeneration, Wnt7a, Extracellular vesicles, Duchenne muscular dystrophy

Background

Wnt7a signaling stimulates muscle regeneration and represents an important intrinsic mechanism for regenerative myogenesis [1, 2]. Wnt7a signaling via the Frizzled7 (Fzd7) receptor activates the planar-cell-polarity (PCP) pathway to drive symmetric expansion of muscle stem cells (MuSCs) and accelerates and augments muscle regeneration [2]. Wnt7a/Fzd7 signaling in myofibers

directly activates the Akt/mTOR growth pathway to induce hypertrophy [3]. Wnt7a/Fzd7 also acts to increase the directional migration of satellite cells and progenitors through activation of the PCP effector proteins Dvl2 and the small GTPase Rac1 [1].

Duchenne muscular dystrophy (DMD) is a devastating muscle wasting disease caused by loss-of-function mutations in the dystrophin gene. Loss of dystrophin in myofibers results contraction-induced damage, increased sarcolemma permeability, cytosolic calcium overloading, oxidative and nitrosamine stress, cell dysfunction, and cell death. Dystrophin is also expressed in MuSCs where it functions to establish polarity which is necessary for efficient asymmetric divisions, and generation of progenitors [4]. Compromised muscle regeneration combined with ongoing muscle damage leads to the progressive disease phenotype in DMD.

*Correspondence:

Michael A. Rudnicki
mrudnicki@ohri.ca

¹Ottawa Hospital Research Institute Regenerative Medicine Program, Ottawa, ON, Canada

²Department of Cellular and Molecular Medicine, Faculty of Medicine, University of Ottawa, Ottawa, ON, Canada

³Electron Microscopy Facility, Centro de Biología Molecular, Severo Ochoa. CSIC, Madrid, Spain

⁴Present address: CIC bioGUNE, Bizkaia Technology Park, Derio 48160, Spain



© The Author(s) 2024. **Open Access** This article is licensed under a Creative Commons Attribution-NonCommercial-NoDerivatives 4.0 International License, which permits any non-commercial use, sharing, distribution and reproduction in any medium or format, as long as you give appropriate credit to the original author(s) and the source, provide a link to the Creative Commons licence, and indicate if you modified the licensed material. You do not have permission under this licence to share adapted material derived from this article or parts of it. The images or other third party material in this article are included in the article's Creative Commons licence, unless indicated otherwise in a credit line to the material. If material is not included in the article's Creative Commons licence and your intended use is not permitted by statutory regulation or exceeds the permitted use, you will need to obtain permission directly from the copyright holder. To view a copy of this licence, visit <http://creativecommons.org/licenses/by-nc-nd/4.0/>.

Wnt7a has been demonstrated to have therapeutic potential as a treatment for DMD [5]. Intramuscular injection (IM) of recombinant Wnt7a protein into the *tibialis anterior* (TA) muscle in *mdx* mice, a mouse model of DMD, results in an increase in muscle mass, and in myofiber hypertrophy, resulting in a doubling in force generation and a 6-fold reduction in myofiber necrosis [5]. These findings suggested that Wnt7a is a promising candidate as an ameliorative therapy for patients with DMD. However, a significant issue in the clinical development of Wnt7a as a therapeutic is that Wnt proteins are highly hydrophobic and thus cannot be delivered via the circulation [6].

We have recently reported that Wnt7a is highly expressed by regenerating myofibers following an acute injury induced by cardiotoxin (CTX) injection where Wnt7a is secreted on the surface of exosomes, a class of small extracellular vesicles (EVs) [7]. Small EVs carry a variety of cargo and thus facilitate the transfer of proteins (e.g. Wnt, HH, Notch), mRNAs, and microRNAs between cells and tissues [8–10]. EVs have been shown to carry Wnts such as Wnt1, Wnt3a, Wnt5a, and Wnt7a on their surface, and efficiently induce Wnt signaling in target cells [7, 11–13], facilitating long-range intercellular communications [14]. Systemic injection of EVs has successfully delivered microRNAs and siRNAs to specific sites, such as the brain or tumors, where gene modulation was documented [15–19]. Therefore, systemic delivery of Wnt7a on EVs represents a potential strategy for stimulating muscle repair in DMD.

In *mdx* mice, muscle regeneration following an acute injury induced by CTX injection results in relatively efficient regeneration associated with an improvement in the muscle phenotype [20]. We hypothesized that the relatively efficient regeneration is due to the high-level induction of endogenous Wnt7a in newly differentiated myofibers that occurs following CTX injury. Therefore, we assessed regeneration following acute injury induced by CTX injection in *mdx* carrying a conditional Wnt7a allele.

We observed a striking deficit in muscle regeneration in mice lacking Wnt7a resulting in reduced muscle function. Similarly to wild type mice, we found that Wnt7a is also secreted at high levels in *mdx* mice in the newly formed regenerating myofibers that arise following an acute muscle injury. Importantly, the deficiency in muscle regeneration in *mdx* muscle lacking Wnt7a could be rescued by a single tail vein injection of a preparation of EVs carrying Wnt7a. Our results indicate that the level of regeneration observed after acute injury of muscle in *mdx* mice is therefore a consequence of high-level expression of endogenous Wnt7a during regenerative myogenesis. Moreover, our experiments suggest that

systemic delivery of Wnt7a-EVs via the circulation represents a potential therapeutic approach for treating DMD.

Results

Wnt7a is required for efficient muscle regeneration in *mdx* mice

We hypothesized that the relatively efficient regeneration in *mdx* muscle following cardiotoxin (CTX)-induced injury is due to the high-level induction of endogenous Wnt7a that occurs in newly differentiated myofibers [2]. Accordingly, we observed high level induction of Wnt7a in newly differentiating myofibers in the *tibialis anterior* (TA) muscles in *mdx* mice at 96 h following CTX injury (Fig. 1A). Non-injected contralateral TA muscles were used as uninjured controls. Therefore, we evaluated regenerating muscle from mice with a functional Wnt7a gene (*Myf5^{Cre/+};Wnt7a^{+/+}*) versus mice where Wnt7a was specifically deleted in muscle (*Myf5^{Cre/+};Wnt7a^{fl/fl}*), in both *C57/BL10* (WT) or *C57BL/10ScSn-Dmd^{mdx}/J* (*mdx*) backgrounds (Fig. 1B). *Myf5-Cre* is expressed from early development, and this facilitates the efficient deletion of floxed alleles in differentiated adult skeletal muscle.

In uninjured TA muscles from WT mice, no significant difference was observed in the numbers of Pax7-expressing cells regardless of whether Wnt7a was deleted (Fig. 1C). WT muscle without Wnt7a exhibited a significant increase in the numbers of Pax7-expressing cells after CTX injury (Fig. 1C and D). In uninjured TA muscles from *mdx* mice lacking Wnt7a, we observed about a 2-fold increase in numbers of Pax7-expressing cells compared to *mdx* mice with a functional Wnt7a gene (Fig. 1E). In contrast to WT mice, deletion of Wnt7a in *mdx* muscle did not result in an increase in numbers of Pax7-expressing satellite cells at 21 d following CTX injection (Fig. 1E and F).

Histological characterization of the uninjured WT TA muscle showed no significant differences upon deletion of Wnt7a expression in the myofiber distribution (Fig. S1A), minimal myofiber Feret average (Fig. S1B), number of fibers (Fig. S1C) or area (Fig. S1D). Conversely, we observed a strong phenotype in injured WT TA muscle sections lacking Wnt7a. Analysis of minimal fiber Feret in the TA at 21d post-CTX revealed a significant shift towards smaller myofibers and a corresponding reduction in larger myofibers in WT mice lacking Wnt7a (Fig. 1G-I and S1E). We also observed a significant increase in the total number of myofibers (Fig. S1F). However, no significant difference was observed in the TA total cross-sectional area (Fig. S1G). Therefore, we conclude that Wnt7a is required for normal progression of muscle regeneration in WT mice.

Strikingly, in *mdx* mice examination of uninjured TA muscle showed a significant increase in the percentage of smaller myofibers in muscles lacking Wnt7a and

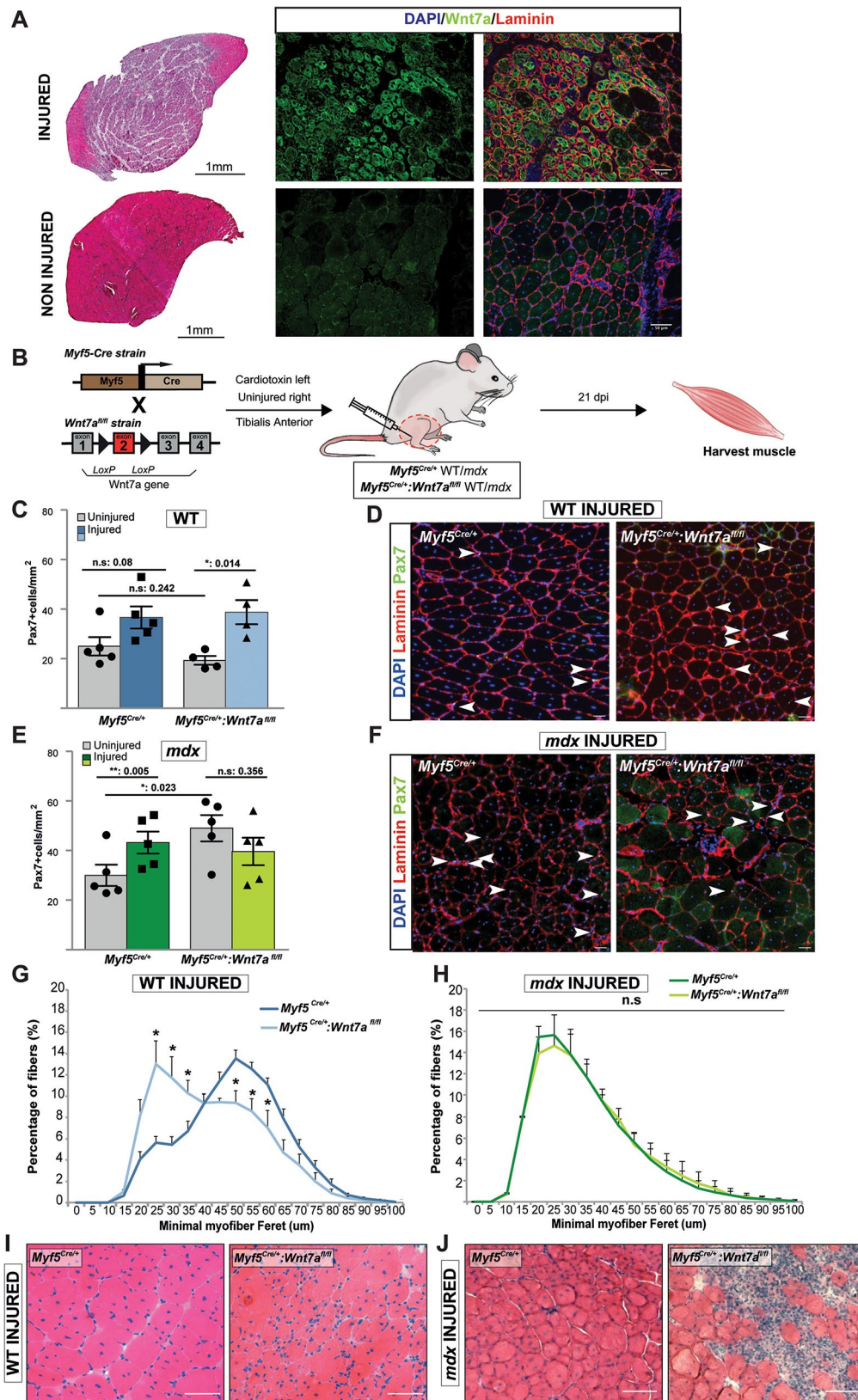


Fig. 1 (See legend on next page.)

(See figure on previous page.)

Fig. 1 Lack of Wnt7a expression impairs muscle regeneration. (A-left) H&E stained sections of injured and non-injured TA muscle of *mdx* mice at 3 dpi. (A-right) Wnt7a immunostained (green) sections of injured and non-injured TA from *mdx* mice upon 3 dpi. Laminin (red) delineates myofibers. Nuclei are stained with DAPI. (B) Mouse strains used and experimental design. (C and D) Quantification of Pax7-expressing cells in regenerating WT muscle. Scale bar 50 μ m. (E and F) Quantification of Pax7-expressing cells in regenerating *mdx* TA muscle. Scale bar 50 μ m. (G and H) Myofiber caliber distribution at 21 d following regeneration in WT and *mdx* TA muscle with and without Wnt7a deletion. (I and J) H&E stained sections at 21 d following regeneration in WT and *mdx* TA muscle with and without Wnt7a deletion. Scale bar 100 μ m. TA (Tibialis Anterior), dpi (days post injury). $n \geq 4$ mice, mean \pm s.e.m., p values determined by two-sided Student's t-test (* $p < 0.05$, ** $p < 0.01$, n.s.=not significant)

a corresponding reduction in larger myofibers (Fig. S1H-I). However, no significant differences were observed in number of fibers (Fig. S1J) or area (Fi. S1K).

Interestingly, examination of TA muscle in *mdx* mice at 21d following CTX-induced injury revealed a similar distribution in myofiber ferret sizes (Fig. 1H), and no significant differences in the average myofiber caliber (Fig. S1L). However, we noted significantly decreased numbers of myofibers present in the regenerated *mdx* muscle lacking Wnt7a (Fig. S1M), but no difference in TA total cross-sectional area (Fig. S1N). Finally, we observed extensive areas of fibrosis that were not evident in regenerated muscles in *mdx* mice with Wnt7a (Fig. 1J).

Overall, these data are consistent with an essential role played by Wnt7a/Fzd7 signaling in stimulating the efficient regeneration of skeletal muscle after an acute injury. Our experiments indicate that in the absence of Wnt7a, the regeneration deficit in dystrophin deficient muscle is exasperated resulting in a significant impairment in the regenerative response.

Reduced force generation in regenerated muscles lacking Wnt7a

To evaluate the functional consequence of a lack of Wnt7a on muscle regeneration, we examined force generation in WT and *mdx* mice that either expressed Wnt7a (*Myf5^{Cre/+}:Wnt7a^{+/+}*), or where Wnt7a had been deleted (*Myf5^{Cre/+}:Wnt7a^{fl/fl}*) (Fig. 2A). In uninjured TA muscles from WT mice, deletion of Wnt7a in muscle did not have a significant effect on specific force generation across the force frequency profile (Fig. 2B). By contrast, in uninjured TA muscles from *mdx* mice lacking Wnt7a, we observed a significant decrease in specific force generation relative to uninjured TA muscles from *mdx* mice expressing endogenous Wnt7a (Fig. 2C).

Examination of force generation in the regenerated TA muscle at 21 d following CTX injury revealed a significant reduction in specific force generation in WT mice lacking Wnt7a (Fig. 2D). This was associated with a significant increase in the weight of the CTX injured TA (Fig. S2A, S2B). These results support the notion that Wnt7a is required for the efficient regeneration of muscle following an acute injury. In *mdx* TA muscle lacking Wnt7a, we observed a significant reduction in specific force generation at 21 d after CTX injection (Fig. 2E). In contrast to WT muscle, no significant change in the weight of the CTX injured TA was observed (Fig. S2C,

S2D). Together, these results support the conclusion that Wnt7a is required for the normal regenerative response following an acute muscle injury in both WT and *mdx* muscle. Furthermore, the reduced force generation in uninjured TA muscles of *mdx* mice lacking Wnt7a argues that Wnt7a is playing a role in slowing the progression of dystrophic disease due to chronic muscle damage in *mdx* mice.

Wnt7a on extracellular vesicles display bioactivity

To assess whether the observed regeneration deficits were indeed due to the deletion of Wnt7a, we performed a rescue experiment where Wnt7a was delivered systemically via tail vein injection of EVs. To evaluate the bioactivity of Wnt7a-EVs on MuSCs, we first asked whether Wnt7a-EVs could stimulate symmetric MuSCs division as previously described using recombinant Wnt7a [2]. Therefore, EVs were isolated from Wnt7a (Wnt7a-EV) and empty vector (CTR-EV) transfected primary myoblasts after three days of differentiation using a tangential flow filtration (TFF) protocol we developed [7] (Fig. S3A). Myotube derived small EVs exhibited the typical size range of between 50 and 200 nm (Fig. S3B). Examination of purified Wnt7a-EVs by immunogold transmission electron microscopy (iTEM) after staining using anti-Wnt7a antibody revealed localization of Wnt7a to the surface of EVs, with the appropriate size and morphology (Fig. S3C). Wnt7a protein content on isolated EVs was quantified using a standard curve of Wnt7a recombinant protein and CD63 as a marker of EVs (Fig. S3D). We observed a content of 2 ng of Wnt7a per ug of total EV protein content based on a standard curve of Wnt7a recombinant protein (Fig. S3D).

Myofibers from the *Flexor Digitorum Brevis* (FDB) muscles were isolated from *Myf5^{Cre/+}:R26R-eYFP* *mdx* mice (Fig. 3A) and cultured in 96-well plates and high content screening performed as previously described [21]. Isolated FDB fibers were treated with 20 ng/ml of Wnt7a equivalents delivered on EVs (Wnt7a-EV), alternatively with recombinant protein (rWnt7a), or also CTR-EVs. FDB myofibers were cultured for 42 h, at which point the majority of muscle stem cells have undergone one round of cell division.

Image analysis was used to quantify the numbers of symmetric and asymmetric satellite stem cell divisions via the expression of eYFP protein (Fig. 3B). The rate of muscle stem cell division was not significantly altered by

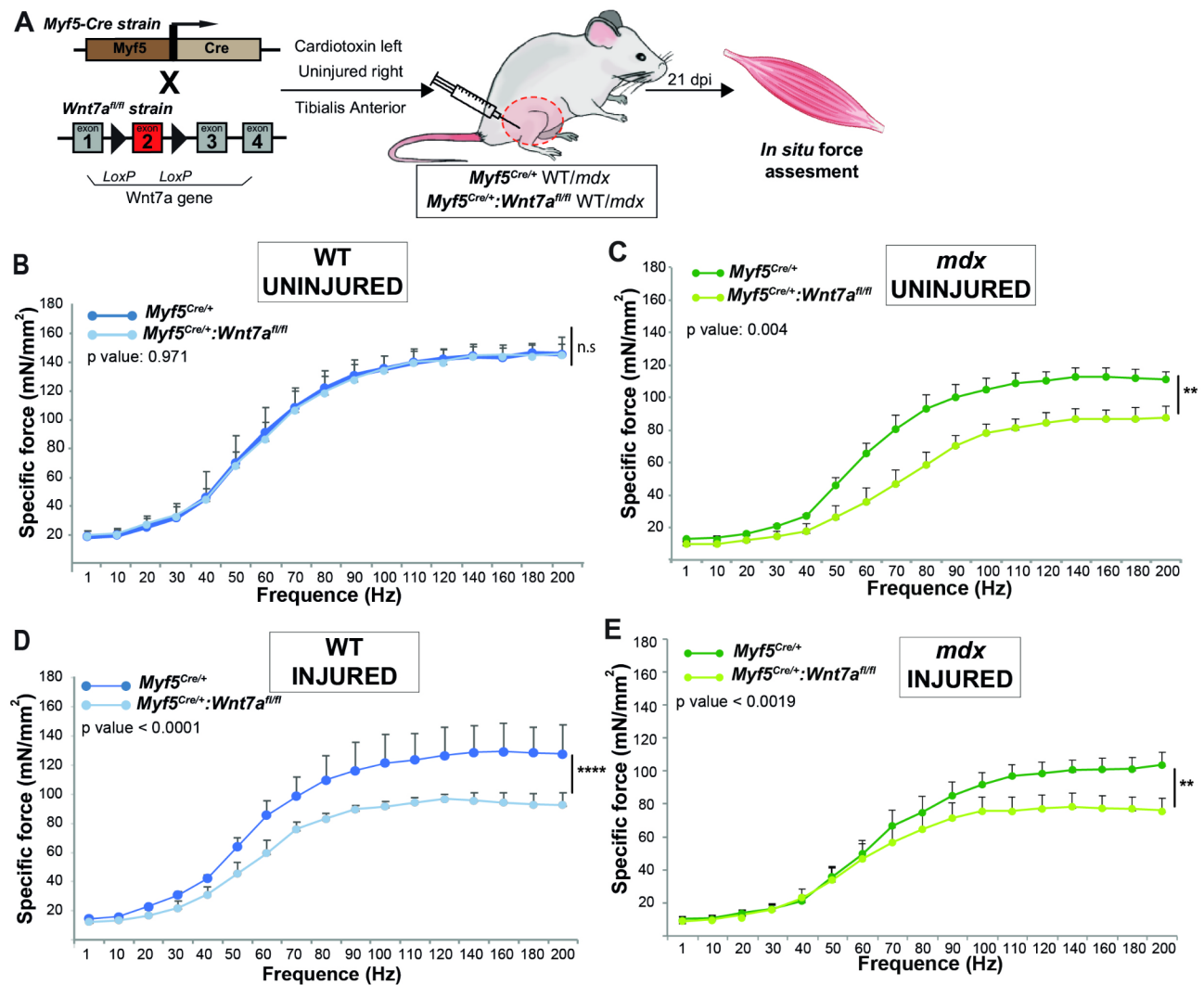


Fig. 2 Reduced force generation in regenerated TA muscles lacking Wnt7a. **(A)** Schematic of mouse strains used and experimental design. **(B)** Specific force frequency curve in uninjured WT TA muscle with (dark blue) and without (light blue) Wnt7a expression. **(C)** Specific force frequency curve in uninjured *mdx* TA muscle with (dark green) and without (light green) Wnt7a expression. **(D)** Specific force frequency curve of regenerated WT TA muscle, with (dark blue) and without (light blue) Wnt7a expression, at 21 d following injury. **(E)** Specific force frequency curve of regenerated *mdx* TA muscle, with (dark green) and without (light green) Wnt7a expression, at 21 d following injury. TA (Tibialis Anterior). n ≥ 3 mice, mean ± s.e.m., p values determined by two-way ANOVA test (*p < 0.05, **p < 0.01, ***p < 0.001, n.s. = not significant)

treatment with either EVs or Wnt7a recombinant protein (Fig. 3C). However, the proportion of symmetric satellite stem cell expansion was significantly increased by Wnt7a-EV or by rWnt7a treatment (Fig. 3D). Interestingly, an equivalent amount of Wnt7a provided on EVs induced significantly more symmetric divisions than rWnt7a suggesting increased bioactivity or bioavailability (Fig. 3D). Therefore, we conclude that Wnt7a carried on EVs isolated from transfected primary myoblasts displays robust bioactivity.

Wnt7a-EVs rescues muscle regeneration in *mdx* mice lacking Wnt7a

To assess whether the regeneration deficit observed in *mdx* mice lacking Wnt7a could be rescued by exogenous Wnt7a, we performed tail vein injections using the preparation of Wnt7a-EVs described above. We first evaluated the biodistribution of Wnt7a-EVs following tail vein injection.

We found that following tail vein injection into WT mice, Wnt7a-EVs exhibited uptake by many different organs including heart, spleen, kidney, and liver (Figure S4A). Notably, uptake into skeletal muscle was markedly increased following CTX injury (Figure Sup 4A). Therefore, we asked whether systemically administered

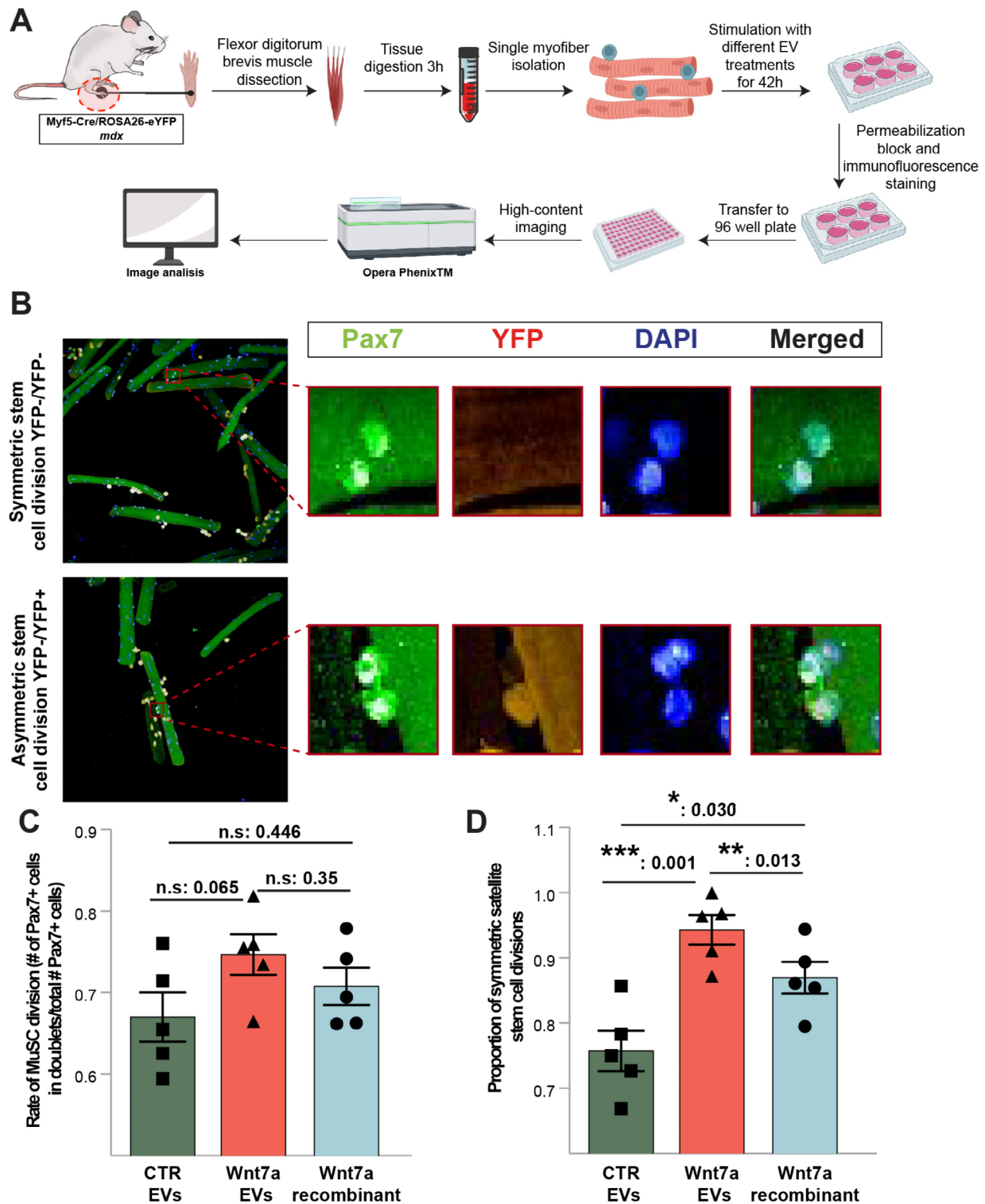


Fig. 3 Wnt7a-EVs exhibit enhanced bioactivity. **(A)** Schematic showing the experimental protocol for ex vivo EV treatment of single myofibers isolated from FDB muscles, imaging and analysis using high-content screening. **(B)** Representative immunofluorescence images of symmetric (top panel) and asymmetric (bottom panel) satellite stem cell divisions. **(C)** Rate of muscle stem cell division after 42 h in culture is not altered by treatment with either Wnt7a-EVs or with recombinant Wnt7a. **(D)** Symmetric satellite stem cell divisions are significantly increased by Wnt7a-EV treatment. EVs (extracellular vesicles), FDB (Flexor Digitorum fibers). $n \geq 5$ replicates, mean \pm s.e.m., p values determined by two-sided Student's test ($*p < 0.05$, $**p < 0.01$, $***p < 0.001$, n.s.=not significant)

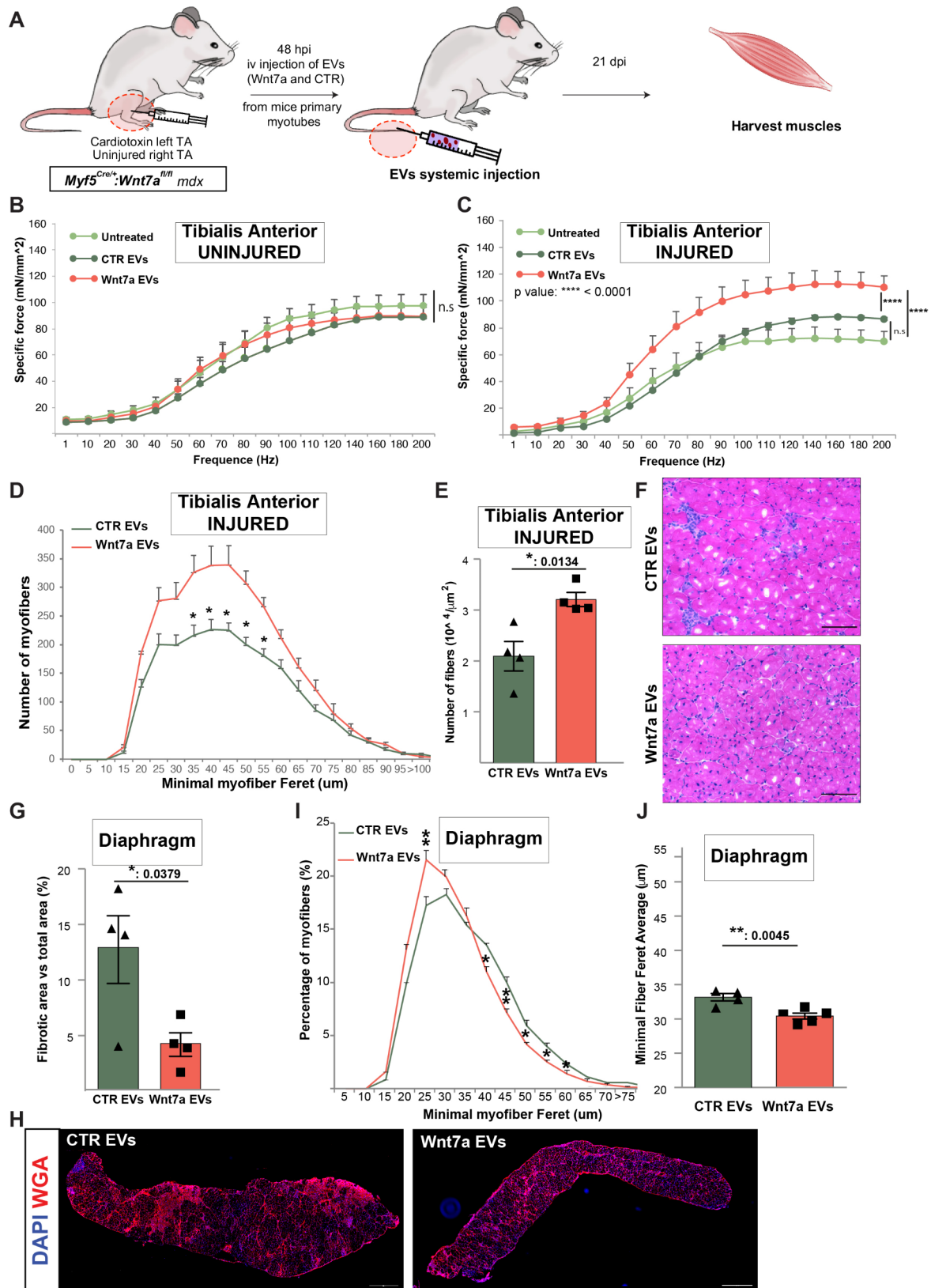


Fig. 4 (See legend on next page.)

(See figure on previous page.)

Fig. 4 Systemic delivery of Wnt7a-EVs rescues muscle regeneration in *mdx* mice. **(A)** Schematic of experimental design. **(B)** Specific Force frequency curve of uninjured *mdx* TA muscle lacking Wnt7a, comparing untreated (light green), control-EV (dark green) injected, or Wnt7a-EV (red) injected. **(C)** Specific Force frequency curve of regenerated *mdx* TA muscle lacking Wnt7a, comparing untreated (light green), control-EV (dark green) injected, or Wnt7a-EV (red) injected. **(D)** Myofiber caliber distribution of regenerated *mdx* TA muscle lacking Wnt7a, comparing control-EV (dark green) injected or Wnt7a-EV (red) injected. **(E)** Wnt7a-EV treatment results in increased numbers of myofibers. **(F)** H&E stained sections of regenerated TA muscles after 21 dpi injected mice with control-EVs or Wnt7a-EVs. Scale bar 100 μ m. **(G)** Quantification of fibrotic area with WGA staining vs. total area in diaphragms showed in % of injected mice with control-EVs or Wnt7a-EVs. **(H)** WGA immunostaining (red) of diaphragm sections from CTR-EV or Wnt7a-EV injected *mdx* mice lacking Wnt7a. Scale bar 500 μ m. **(I)** Myofiber caliber distribution of diaphragms from *mdx* mice lacking Wnt7a injected with control-EVs or Wnt7a-EVs **(J)** Minimal fiber feret average in diaphragms of injected mice with control-EVs or Wnt7a-EVs. TA (Tibialis Anterior), dpi (days post injury, n \geq 4 mice, mean \pm s.e.m., p values determined by two-way ANOVA or two-sided Student's test (* $p < 0.05$, ** $p < 0.01$, **** $p < 0.0001$, n.s.=not significant)

Wnt7a-EVs delivered by tail vein injection could ameliorate the dystrophic phenotype in *mdx* mice upon acute injury (Fig. 4A). For these experiments, we made use of *mdx: Myf5^{Cre/+}; Wnt7a^{fl/fl}* mice as a sensitized model to assess Wnt7a activity.

The TA muscles of *mdx* mice lacking Wnt7a were injured by CTX injection and a single dose of Wnt7a-EV or CTR-EV delivered by tail vein injection at 48 h post injury (Fig. 4A). The total dose of Wnt7a protein delivered amounted to 700 ng. Muscle force determination and histological assessments were performed at 21 days post injury. In uninjured TA muscles, we observed no change in the force frequency profile (Fig. 4B). Remarkably, systemic delivery of Wnt7a-EVs in injured TA muscle had a significant positive effect on the force frequency profile compared to CTR-EVs treatment (Fig. 4C).

Histological characterization of the entire injured TA muscle sections (Fig. S4B) upon systemic treatment with Wnt7a EVs or CTR EVs showed no differences in the distribution of myofiber caliber size (Fig. 4D), average caliber (Fig. S4C) or total cross-sectional area (Fig. S4D). However, systemic treatment with Wnt7a EVs revealed a significant increase in the number of myofibers compared to CTR-EVs consistent with a stimulation of the regenerative response (Fig. 4E). Accordingly, H&E results reflected a better myoregenerative outcome with fewer fibrotic areas after systemic treatment with Wnt7a-EVs relative to CTR-EVs (Fig. 4F). Lastly, no significant difference in Pax7 numbers were found in the treated TA muscle perhaps reflecting the point that a single dose of Wnt7a was delivered 21 days prior to sacrifice allowing a return to homeostasis (Fig. S4E-F).

We lastly asked within the same experiment whether the myoregenerative effect after systemic delivery of Wnt7a-EVs was also stimulating regeneration in the diaphragm. Histological analysis of the diaphragm comparing Wnt7a-EV and CTR-EV treated *mdx: Myf5^{Cre/+}; Wnt7a^{fl/fl}* mice revealed an overall improvement of the histopathological presentation of the diaphragm condition after treatment Wnt7a-EVs with reduced fibrotic infiltration (Fig. 4G-H and S4G). The distribution of myofiber caliber size (Feret's diameter) showed a significant shift towards the formation smaller regenerating myofibers after treatment with Wnt7a-EVs

(Fig. 4I-J and S4H). Interestingly, the effect of Wnt7a-EV on the diaphragm suggests that EV uptake can readily occur in dystrophic muscles.

All together, these data indicate that Wnt7a-EVs delivered systemically via the circulation positively stimulates regeneration of dystrophic skeletal muscle.

Discussion

We have discovered that Wnt7a expression in muscle is required for an efficient regenerative response following an acute injury in muscle. Moreover, we observed reduced force generation in muscle of *mdx* mice as well as reduced regenerative capability following an acute injury. The muscle regeneration deficit was rescued by a single tail vein injection of a preparation of Wnt7a-EVs. Therefore, we conclude that intrinsic Wnt7a secretion by myofibers plays an important role in muscle homeostasis and regeneration. Furthermore, our experiments open new therapeutic avenues to develop systemic treatments for Wnt7a therapy for the treatment of DMD.

The lack of Wnt7a expression in WT versus dystrophic muscle has different consequences on the regenerative response. We found that deletion of Wnt7a in WT muscle fibers appeared to delay the myoregenerative response. After acute injury, we observed an increase in Pax7-expressing myogenic cells, no change in the number of myofibers, but a marked reduction in average myofiber caliber, resulting in reduced force generation. By contrast, the deletion of Wnt7a in *mdx* muscle resulted in a severely reduced regenerative response. We observed reduced numbers of Pax7-expressing cells, reduced numbers of myofibers, and a poor overall regenerative response resulting in a decreased ability to generate force. Interestingly, we observed that in WT muscle lacking Wnt7a, the muscle weight was increased following injury. Conversely, in *mdx* muscle we observed no difference. We speculate that this may be a consequence of compensatory factors acting on the progenitors during regeneration, perhaps involving other Wnts or secreted factors. The intrinsic deficits in asymmetric division leading to reduced generation of progenitors in *mdx* muscle potentially blunts these compensatory mechanisms. Together, our experiments support the notion that the relatively efficient regeneration induced by CTX-injection in *mdx*

muscle is a consequence of high-level upregulation of Wnt7a.

The increase in numbers of Pax7-expressing cells in WT but not in *mdx* muscle following an acute injury suggests that the perturbations of dystrophin-deficient satellite cell function are an important aspect to consider. Dystrophin is highly expressed in newly activated satellite cells where it establishes apical-basal polarity which is necessary for efficient asymmetric divisions, and generation of progenitors [4]. Both *mdx* and DMD muscle exhibit a hyperplasia of the muscle stem cell compartment with a 3–5 fold increase in the numbers of Pax7-expressing cells at all stages of the disease [22]. It is interesting to speculate that the increase in numbers of WT muscle lacking Wnt7a is a consequence of continued proliferation of progenitors due delayed regeneration. In *mdx* muscle lacking Wnt7a, the Pax7-expressing cells are not generating sufficient progenitors for this response to occur, as evidenced by the marked reduction in the numbers of regenerated myofibers. Likewise, these findings are supported by a growing body of evidence that supports the contention that muscle regeneration is delayed in *mdx* mice due to intrinsic deficits in MuSC function resulting in reduced generation of progenitors [4, 23]. Further experiments, including single cell RNA-seq would elucidate these phenomena.

Previously, we have shown that endogenous Wnt7a is secreted at high levels in vivo on the surface of EVs in regenerating myofibers following an acute injury [7]. To generate Wnt7a-EVs for use in our experiments, we expressed Wnt7a in primary myoblasts, then induced differentiation into myotubes to facilitate isolation of Wnt7a-EVs from conditioned using TFF. We found that Wnt7a-EVs exhibited robust bioactivity when we assessed their ability to stimulate symmetric satellite stem cell divisions on cultured myofibers. The enhanced activity of Wnt7a-EVs relative to recombinant Wnt7a may reflect the short half-life of recombinant Wnt7a [24]. Alternatively, Wnt7a-EVs may display enhanced bioactivity due to their inherent capacity to facilitate long-range signaling [15–17].

We found that a single injection of Wnt7a-EVs via the tail vein in *mdx* mice lacking Wnt7a rescued their regeneration deficit. Notably, Wnt7a-EV injection resulted in a marked increase in specific force generation compared to mice injected with CTR-EVs. Strikingly, the observed specific generation reaches the same levels as WT muscle following injury. Histological analysis revealed a remarkable improvement in the histopathological appearance of the muscle. Importantly, we confirm that Wnt7a-EVs treatment via intravenous injection represents an efficient systemic treatment to treat the entire body, as histological results from the diaphragm revealed an enhancement of the regenerative response.

Overall, we have demonstrated that Wnt7a is required for efficient muscle regeneration following an acute injury in muscle. Our experiments further reveal a role for endogenous Wnt7a in slowing the progression of dystrophic disease by stimulating regeneration. We have shown that Wnt7a-EVs can be delivered via the circulation to rescue the regeneration phenotype in *mdx* mice lacking Wnt7a. This innovation overcomes the hydrophobicity limitation that characterized Wnt7a free soluble protein, which could only be delivered by intramuscular injection [5]. Taken together, our findings suggest that Wnt7a loaded into small EVs represents a potential systemic delivery strategy to stimulate skeletal muscle regeneration in all muscle groups throughout the body toward ameliorating dystrophic progression in Duchenne muscular dystrophy.

Materials and methods

Mice and animal care

All experimental protocols for mice used in this study were approved by the University of Ottawa Animal Care Committee, which is based on the guidelines of the Canadian Council on Animal Care. Food and water were administered *ad libitum*. Muscle regeneration experiments were assessed in 12-week-old male obtained from F2 cross between the offspring of *Myf5-Cre* mice [25] and *Wnt7a^{fl/fl}* mice [26] in a C57BL/6 genetic background or *C57BL/10ScSn-Dmd^{mdx}/J* genetic background. In Figs. 1 and 2 muscle regeneration experiments were performed as previously described [27] with the following modifications. Mice were anesthetized with isoflurane and CTX injection was performed on a single injection into the TA (50 μ l, 10 μ M) and muscle regeneration assessed after 21 days.

Immunohistochemistry

TA and diaphragm muscle cryosections were rehydrated using PBS, and then fixed with 2% PFA in PBS at room temperature. After washing with PBS, permeabilization with a solution of 0.1% Triton and 0.1 M glycine in PBS was applied for 10 min at room temperature. Mouse on mouse blocking reagent was used at a dilution of 1:40 in blocking solution of 10% goat serum, 1% bovine serum albumin (BSA) and 0.1% Tween 20 in PBS for one hour at room temperature. Primary antibodies were incubated overnight. Nuclei were counterstained with DAPI before mounting in Permafluor. For analysis Z-stack images of cryosections were acquired on an epifluorescence microscope equipped with a motorized stage (Zeiss AxioObserver Z1) with a step size of 0.2 μ m to span the cell (25 slices in total) and images were deconvoluted using Zen Software (Zeiss). 3D sum intensity Z-projection was performed with ImageJ software. Laminin staining was analyzed for fiber counting and minimum Feret's diameter

using SMASH [28]. Antibodies and dilutions are provided in Table S1.

In-situ TA muscle force measurements

In-situ TA muscle function (twitch and tetanic force) was evaluated according to previously published protocols [29, 30]. Experimental mice were anesthetized with 2–5% vaporized isoflurane mixed with O₂. The distal TA tendon and TA muscle were exposed, and the mouse was transferred to an in-situ mouse apparatus with a temperature-controlled footplate platform. The mouse was positioned on a heated surface to maintain the body and muscle temperature at 37°C. The knee was secured to a fixed steel post using surgical sutures and the foot was pinned to the platform to prevent movement from contraction of other muscle groups. The distal tendon of the TA muscle was attached to FT03 force transducers connected to a 79E physiograph (Grass Technologies, Warwick, U.S.A.), which in turn was connected to a KCP13104 data acquisition system (Keithley, U.S.A.). Exposed muscles were kept from drying out using physiological saline solution (118.5 mM NaCl, 4.7 mM KCl, 2.4 mM CaCl₂, 3.1 mM MgCl₂, 25 mM NaHCO₃, 2 mM NaH₂PO₄, and 5.5 mM D-glucose). Electrical stimulations were applied with two needle electrodes that were placed through the skin just above and below the knee to stimulate the tibial nerve. The electrodes were connected to a Grass S88 stimulator and a Grass SIU5 isolation unit (Grass Technologies). Tetanic contractions were elicited every 100 s with 200 ms trains of 0.3 ms, 5 V (supramaximal voltage) pulses at frequencies ranging from 1 to 200 Hz. Absolute tetanic force was defined as the force generated upon stimulation and calculated as the difference in force at the maximum height of contraction and the force just prior to the stimulation. The specific muscle force was calculated by dividing the absolute muscle force by the muscle cross-sectional area (CSA). Muscle CSA was calculated according to the following equation: CSA = (muscle length in cm / muscle weight in g) * TA muscle density, which was considered to be 1.06 g/cm³.

Cell culture

Wnt7a expressing primary myoblasts were obtained upon infection of primary myoblasts from C57BL/10ScSn M1 male mice, previously isolated as Sincennes et al. [31] described. Briefly, myoblasts passage 4 were seeded in 6-well plate (1.0 × 10⁵ cells/well/4 ml media) and infected with lenti-III-Ubc-Wnt7a lentivirus (30 μl virus/well) created in our laboratory, empty vector lentivirus as control, containing 6 μg/ml Polybrene in 1.5 ml culture media (Collagen-coated dishes with HAM F12-X, 10% FBS, 100 U/mL penicillin, 100 U/mL streptomycin and maintained at 37 °C in a humidified incubator equilibrated with 5% CO₂). Selection was done with Puromycin (2.5 μg/mL)

to establish the stable cell line. Six different colonies were picked and Wnt7a expression was verified by immunoblot. Primary myoblasts were cultured on collagen-coated dishes with HAM F12-X, 10% FBS, 100 U/mL penicillin, 100 U/mL streptomycin and maintained at 37 °C in a humidified incubator equilibrated with 5% CO₂.

Conditioned media production for cell derived EVs

For EVs derived from Wnt7a expressing primary myotubes, equal numbers of cells were seeded and let them grow in growth media. For differentiation, myoblasts were grown up to 80% confluence and growth media was replaced with differentiation medium [HAM F12-X: DMEM (1:1), 5% HS, 100 U/mL penicillin, and 100 U/mL streptomycin] for 3d maintained at 37 °C in a humidified incubator equilibrated with 5% CO₂. Before differentiation serum was pre-cleared of free of extracellular vesicles as previously stated [32]. Then media was collected for EVs isolation following regular protocol.

EV isolation

Conditioned media (20 mL) was clarified by sequential centrifugation (300 g at RT for 10 min; 2500 g at RT for 10 min and 20,000 g at 4 °C for 20 min). Supernatant was transferred to Flexboy bag (Sartorius) and subjected to tangential flow filtration (TFF) under sterile conditions. Briefly, a KrosFlo Research 2i TFF system (Spectrum Laboratories) coupled to a MidGee Hoop ultrafiltration hollow fiber cartridge (GE Healthcare) 500-KDa MWCO was used. Transmembrane pressure was automatically adjusted at 3 PSI and a shear rate at 3000 s⁻¹. Sample was concentrated up to 10 mL and then subjected to continuous diafiltration. Finally, sample was concentrated at 5 mL and recovered from the cartridge. Lastly, EVs were pellet down after spinning on an ultrabench centrifuge for 30 min at 100,000 g at 4 °C.

Immunogold labeling of EVs

Electron microscopy EV analysis was performed according to the to the protocol previously described by Carrasco-Martinez et al. [33]. Briefly, myotube derived EVs were deposited on colloidal and coated grids and immunolabeled with anti-Wnt7a antibody (R&D Systems). First grids were incubated with 0.1% saponine in PBS for 5 min and blocked with 10% fetal bovine serum for 10 min. Incubation with the antibody was performed for 45 min at room temperature followed by rabbit anti-goat antibodies conjugated to 15 nm gold particles (BBI international) for 30 min. Finally, grids were washed several times with PBS and double distilled water and negative stained with 1% uranyl acetate in water for 40 s. Grids were visualized in a JEM1400 Flash (Jeol, Japan) at 100 kV accelerating voltage and a CMOS 4 K × 4K OneView de Gatan camera (Warrendale, PA, USA).

Immunoblot analysis

Immunoblot analysis was performed as described previously [34] with the following modifications. The lysates from EVs were not clarified by centrifugation. The immunoblot transferring was performed onto PVDF membranes. Antibodies and dilutions are provided in Table S1.

FDB myofiber assay

Single myofibers were isolated from the flexor digitorum brevis (FDB) muscles of 8-week old *mdx* Myf5-Cre/R26R-eYFP mice according to our published protocol [21]. Following dissection, FDB muscles were incubated in DMEM with 2% L-glutamine, 4.5% glucose, and 110 mg/mL sodium pyruvate (GIBCO) containing 0.2% collagenase I (Sigma) for 3 h at 37°C with periodic agitation. Myofibers were isolated using gentle trituration in DMEM+with 2% L-glutamine, 4.5% glucose, and 110 mg/ml sodium pyruvate (GIBCO) containing 20% FBS (Wisent) with a glass pipet. They were then cultured at 37°C in suspension in 24-well plates containing DMEM+with 2% L-glutamine, 4.5% glucose, and 110 mg/ml sodium pyruvate (GIBCO) containing 20% FBS (Wisent) and 1% chick embryo extract (CEE, Accurate Chemicals), and supplemented with different EVs stimulus, expressing Wnt7a or empty vector. EVs concentration was equal to 10 mg/mL of total protein, previously measured with Bradford, accordingly to manufacturer's instructions. On the case of Wnt7a EVs, 10 mg/mL of total protein is equal to 20ng/mL of Wnt7a, based on our quantifications using a standard curve with Wnt7a recombinant protein (Fisher). We have used as a positive control Wnt7a recombinant protein at 100 ng/ml. After 42 h in culture, fibers were fixed and stained for Pax7, YFP, and DAPI as previously described [21]. Fibers were then transferred to 96-well culture plates and scanned and imaged using the Opera-Phenix high-content screening system, equipped with the Columbus processing and analysis software, which enabled the quantification of satellite cell progenitor and stem cell divisions using an automated approach to reduce bias [21].

Systemic EVs treatment

All experimental protocols for mice used in this study were approved by the University of Ottawa Animal Care Committee, which is based on the guidelines of the Canadian Council on Animal Care. Food and water were administered *ad libitum*.

For Figure supplemental 4A muscle regeneration experiments were assessed in 12-week-old male C57BL mice. Muscle regeneration experiments were performed as previously described [27] with the following modifications. Mice were anesthetized with isoflurane and CTX injection was performed on a single injection into the

TA (50 μ l, 10 μ M). 48 h post injury mice were tail vein injected with 25uL saline solution containing myotube derived-EVs, expressing empty vector and labeled with the red fluorescence lipophilic dye PKH26, following manufacturer's instructions. Twenty minutes post injection mice were sacrificed and the different organs were harvested and fluorescence was visualized with an optical imager (IVIS Spectrum).

For Fig. 4A-I and Figure supplemental 4B-H muscle regeneration experiments were assessed in 12-week-old male obtained from F2 cross between the offspring of *Myf5-Cre* mice [25] and *Wnt7a^{fl/fl}* mice [26] in a C57BL/10ScSn-Dmd^{*mdx*}/J genetic background. Muscle regeneration experiments were performed as previously described [27] with the following modifications. Mice were anesthetized with isoflurane and CTX injection was performed on a single injection into the TA (50 μ l, 10 μ M). 48 h post injury mice were tail vein injected with 25uL saline solution containing myotube derived-EVs, expressing empty vector or Wnt7a and muscle regeneration was assessed after 21 days. Dose was calculated previously in a dose-response assay (data not showed) based on the minimal dose to trigger a regenerative response measured by physiology muscle force assay. Intravenously injected solution of EVs contained 350ug of total protein that equals 430 ng of Wnt7a protein measured by immunoblot, using Wnt7a recombinant protein for the standard curve and diluted in 300uL of saline. Equal volumes and protein concentration were injected for empty vector EVs and Wnt7a EVs.

Statistical analysis

Experiments were performed with a minimum of three biological replicates and results are presented as the mean \pm SEM. Student's t-test were performed to assess the statistical significance of two-tailed analysis. For multiple comparisons ANOVA test was employed and TUKEY test for post-hoc analysis. *P*-values are indicated as **p* \leq 0.05, ***p* \leq 0.01, ****p* \leq 0.001, and *P*-values $<$ 0.05 were considered statistically significant. The exact *p* values are shown in each figure.

Supplementary Information

The online version contains supplementary material available at <https://doi.org/10.1186/s13395-024-00367-x>.

Supplementary Material 1

Acknowledgements

The authors thank Dr. Thomas Spencer for providing the floxed Wnt7a mice and Jennifer Richie for mouse colony management.

Author contributions

UGR, KK, and MAR designed research; UGR, K, DD, EJ, FX, and MTR performed research; UGR, KK, DD, EJ, FX and MAR analyzed data, and UGR, KK and MAR wrote the paper.

Funding

This study was supported by Defeat Duchenne Canada, the US National Institutes for Health [R01AR044031], the Canadian Institutes for Health Research [FDN-148387; PJT-183804], Ontario Institute for Regenerative Medicine, and the Stem Cell Network. D.D. held a Frederick Banting and Charles Best Canada Graduate Scholarships - Doctoral Award (CGS-D).

Data availability

Access to primary data and experimental resources is available on request.

Declarations

Animal ethics approval

Housing, husbandry, and all experimental protocols for mice used in this study were performed in accordance with the guidelines established by the University of Ottawa Animal Care Committee, which is based on the guidelines of the Canadian Council on Animal Care. Committee's reference number: 1. OHRle-3868 - Experimental Protocol - Genetic Mouse Models for Investigating the Molecular Mechanisms of Muscle Regeneration [Expires June 30th, 2026]. 2. OHRlb-3826 - Breeding Protocol - Genetic Mouse Models for Investigating the Molecular Mechanisms of Muscle Regeneration [Expires March 31st, 2026].

Consent for publication

Not applicable.

Competing interests

MAR is a co-inventor on patents pertaining to the use of Wnt7a to enhance muscle regeneration. The remaining authors declare no conflict of interest.

Received: 10 June 2024 / Accepted: 4 December 2024

Published online: 19 December 2024

References

- Bentzinger CF, von Maltzahn J, Dumont NA, Stark DA, Wang YX, Nhan K, et al. Wnt7a stimulates myogenic stem cell motility and engraftment resulting in improved muscle strength. *J Cell Biol*. 2014;205:97–111. <https://rupress.org/jcb/article/205/1/97/37610/Wnt7a-stimulates-myogenic-stem-cell-motility-and>
- Le Grand F, Jones AE, Seale V, Scimè A, Rudnicki MA. Wnt7a activates the Planar Cell Polarity Pathway to drive the symmetric expansion of Satellite Stem cells. *Cell Stem Cell*. 2009;4:535–47.
- von Maltzahn J, Bentzinger CF, Rudnicki MA. Wnt7a-Fzd7 signalling directly activates the Akt/mTOR anabolic growth pathway in skeletal muscle. *Nat Cell Biol*. 2012;14:186–91. <http://www.nature.com/glibproxy.wakehealth.edu/ncbjournal/v14/n2/full/ncb2404.html>
- Dumont NA, Wang YX, von Maltzahn J, Pasut A, Bentzinger CF, Brun CE, et al. Dystrophin expression in muscle stem cells regulates their polarity and asymmetric division. *Nat Med*. 2015;21:1455–63.
- von Maltzahn J, Renaud J-MM, Parise G, Rudnicki MA. Wnt7a treatment ameliorates muscular dystrophy. *Proc Natl Acad Sci USA*. 2012;109:20614–9. <http://www.pubmedcentral.nih.gov/articlerender.fcgi?artid=3528612&tool=pmcentrez&rendertype=abstract%5Cn>. <https://www.scopus.com/inward/record.url?eid=2-s2.0-84874422456&partnerID=40&md5=9cabbb66e35a1e8f6e14ba7a7c05ddc8>
- Janda CY, Waghray D, Levin AM, Thomas C, Garcia KC. Structural basis of Wnt recognition by frizzled. *Science*. 2012;336:59–64.
- Gurriaran-Rodriguez U, De Repentigny Y, Kothary R, Rudnicki MA. Isolation of small extracellular vesicles from regenerating muscle tissue using tangential flow filtration and size exclusion chromatography. *Skelet Muscle*. 2024;14(1):22. <https://doi.org/10.1186/s13395-024-00355-1>
- Van Niel G, D'Angelo G, Raposo G. Shedding light on the cell biology of extracellular vesicles. *Nat Rev Mol Cell Biol*. 2018;19:213–28. <https://doi.org/10.1038/nrm.2017.125>
- Kalluri R, LeBleu VS. The biology, function, and biomedical applications of exosomes. *Science* (1979). 2020;367.
- García-Silva S, Benito-Martín A, Nogués L, Hernández-Barranco A, Mazariegos MS, Santos V, et al. Melanoma-derived small extracellular vesicles induce lymphangiogenesis and metastasis through an NGFR-dependent mechanism. *Nat Cancer*. 2021;2:1387–405.
- Gross JC, Chaudhary V, Bartscherer K, Boutros M. Active Wnt proteins are secreted on exosomes. *Nat Cell Biol*. 2012;14:1036–45. <https://doi.org/10.1038/ncb2574>
- Menck K, Klemm F, Gross JC, Pukrop T, Wenzel D, Binder C. Induction and transport of Wnt 5a during macrophage-induced malignant invasion is mediated by two types of extracellular vesicles. *Oncotarget*. 2013;4:2057–66. <http://www.pubmedcentral.nih.gov/articlerender.fcgi?artid=3875769&tool=pmcentrez&rendertype=abstract>
- Dziadlo E, Rudnik M, Koning R, Czepiel M, Tkacz K, Baj-Krzyworozeka M, et al. WNT3a and WNT5a transported by exosomes activate WNT signaling pathways in human cardiac fibroblasts. *Int J Mol Sci*. 2019;20:1436.
- van Niel G, Carter DRF, Clayton A, Lambert DW, Raposo G, Vader P. Challenges and directions in studying cell–cell communication by extracellular vesicles. *Nat Rev Mol Cell Biol*. 2022;23:369–82.
- Beckett K, Monier S, Palmer L, Alexandre C, Green H, Raposo G et al. Europe PMC Funders Group Drosophila Wingless is loaded on exosome-like vesicles but forms a gradient in an exosome-independent manner. 2015;14:82–96.
- Alvarez-Erviti L, Seow Y, Yin H, Betts C, Lakhal S, Wood MJA. Delivery of siRNA to the mouse brain by systemic injection of targeted exosomes. *Nat Biotechnol*. 2011;29:3–4. <https://doi.org/10.1038/nbt.1807>
- Ohno S, Takanashi M, Sudo K, Ueda S, Ishikawa A, Matsuyama N et al. Systemically Injected Exosomes Targeted to EGFR Deliver Antitumor MicroRNA to Breast Cancer Cells. *Molecular Therapy*. 2013;21:185–91. <https://doi.org/10.1038/mt.2012.180>
- Liu Y, Li D, Liu Z, Zhou Y, Chu D, Li X, et al. Targeted exosome-mediated delivery of opioid receptor Mu siRNA for the treatment of morphine relapse. *Sci Rep*. 2015;5:17543. <http://www.pubmedcentral.nih.gov/articlerender.fcgi?artid=4668387&tool=pmcentrez&rendertype=abstract>
- Nakayama F, Miyoshi M, Kimoto A, Kawano A, Miyashita K, Kamoshida S, et al. Pancreatic cancer cell-derived exosomes induce epithelial-mesenchymal transition in human pancreatic cancer cells themselves partially via transforming growth factor β 1. *Med Mol Morphol*. 2022;55:227–35.
- Pessina P, Cabrera D, Morales MG, Riquelme CA, Gutiérrez J, Serrano AL, et al. Novel and optimized strategies for inducing fibrosis in vivo: focus on Duchenne muscular dystrophy. *Skelet Muscle*. 2014;4:7.
- Chen WY, Perkins TJ, Rudnicki MA. Quantification of Muscle Satellite Stem Cell Divisions by High-Content Analysis. 2023. pp. 537–53. https://link.springer.com/https://doi.org/10.1007/978-1-0716-2772-3_29
- Dumont NA, Rudnicki MA. Targeting muscle stem cell intrinsic defects to treat Duchenne muscular dystrophy. *NPJ Regen Med*. 2016;1:16006. <http://www.nature.com/articles/npjregenmed20166>
- Chang NC, Sincennes M-C, Chevalier FP, Brun CE, Laciaia M, Segalés J, et al. The Dystrophin Glycoprotein Complex regulates the epigenetic activation of muscle stem cell commitment. *Cell Stem Cell*. 2018;22:755–e7686.
- Vallon M, Yuki K, Nguyen TD, Chang J, Yuan J, Siepe D, et al. A RECK-WNT7 receptor-ligand interaction enables isoform-specific regulation of Wnt bio-availability. *Cell Rep*. 2018;25:339–349.e9. <https://doi.org/10.1016/j.celrep.2018.09.045>
- Kuang S, Kuroda K, le Grand F, Rudnicki MA. Asymmetric Self-Renewal and Commitment of Satellite Stem cells in muscle. *Cell*. 2007;129:999–1010.
- Dunlap KA, Filant J, Hayashi K, Iii EBR, Song G, Deng JM et al. Postnatal deletion of Wnt7a inhibits uterine gland morphogenesis and compromises adult fertility in mice 1. 2011;396:386–96.
- Gurriarán-Rodríguez U, Santos-Zas I, Al-Massadi O, Mosteiro CS, Beiroa D, Nogueiras R, et al. The obestatin/GPR39 system is up-regulated by muscle injury and functions as an autocrine regenerative system. *J Biol Chem*. 2012;287:38379–89.
- Smith LR, Barton ER. SMASH - semi-automatic muscle analysis using segmentation of histology: a MATLAB application. *Skelet Muscle*. 2014;4.
- Shin J-H, Pan X, Hakim CH, Yang HT, Yue Y, Zhang K, et al. Microdystrophin ameliorates muscular dystrophy in the Canine Model of Duchenne muscular dystrophy. *Mol Ther*. 2013;21:750–7.
- Wang YX, Feige P, Brun CE, Hekmatnejad B, Dumont NA, Renaud J-M, et al. EGFR-Aurka Signaling rescues polarity and regeneration defects in Dystrophin-Deficient muscle stem cells by increasing asymmetric divisions. *Cell Stem Cell*. 2019;24:419–e4326.
- Sincennes MC, Wang YX, Rudnicki MA. In: Perdiguer E, Cornelison DDW, editors. Primary mouse myoblast purification using magnetic cell separation BT - muscle stem cells: methods and protocols. New York, NY: Springer New York; 2017. pp. 41–50.

32. Théry C, Amigorena S, Raposo G, Clayton A. Isolation and Characterization of Exosomes from Cell Culture Supernatants. *Curr Protoc Cell Biol.* 2006;3:3.22.1–3.22.29.
33. Carrasco-Ramírez P, Greening DW, Andrés G, Gopal SK, Martín-Villar E, Renart J, et al. Podoplanin is a component of extracellular vesicles that reprograms cell-derived exosomal proteins and modulates lymphatic vessel formation. *Oncotarget.* 2016;7:16070–89.
34. Gurriarán-Rodríguez U, Santos-Zas I, González-Sánchez J, Beiroa D, Moresi V, Mosteiro CS et al. Action of obestatin in skeletal muscle repair: stem cell

expansion, muscle growth, and microenvironment remodeling. *Mol Ther.* 2015;23.

Publisher's note

Springer Nature remains neutral with regard to jurisdictional claims in published maps and institutional affiliations.